Structure, Vol. 10, 811–823, June, 2002, ©2002 Elsevier Science Ltd. All rights reserved. PII S0969-2126(02)00777-3

The Ig-like Structure of the C-Terminal Domain of Lamin A/C, Mutated in Muscular Dystrophies, Cardiomyopathy, and Partial Lipodystrophy

Isabelle Krimm,[1] Cecilia Östlund,[2] Bernard Gilquin,[1] Joël Couprie,[1] Paul Hossenlopp,[3] Jean-Paul Mornon,[3] Gisèle Bonne,[4] Jean-Claude Courvalin,[5] Howard J. Worman,[2] and Sophie Zinn-Justin[1,6]

[1]Département d'Ingénierie et d'Etudes des Protéines
CEA Saclay
91191 Gif-sur-Yvette
France

[2]Departments of Medicine and Anatomy and Cell Biology
College of Physicians and Surgeons
Columbia University
New York, New York 10032

[3]Laboratoire de Minéralogie-Cristallographie Paris
CNRS UMR 7590
Universités Paris 6/Paris 7
Case 115
4 place Jussieu
75252 Paris Cedex 05
France

[4]INSERM UR523
Institut de Myologie
Bâtiment Babinski
Groupe Hospitalier La Pitié-Salpetrière
47 boulevard de l'Hopital
75651 Paris Cedex 13
France

[5]Département de Biologie Cellulaire
Institut Jacques Monod
Université Paris 7
Tour 43
2 place Jussieu
75251 Paris Cedex 05
France

Summary

Lamins are nuclear intermediate filaments that, together with lamin-associated proteins, maintain nuclear shape and provide a structural support for chromosomes and replicating DNA. We have determined the solution structure of the human lamin A/C C-terminal globular domain which contains specific mutations causing four different heritable diseases. This domain encompasses residues 430–545 and adopts an Ig-like fold of type s. We have also characterized by NMR and circular dichroism the structure and thermostability of three mutants, R453W and R482W/Q, corresponding to "hot spots" causing Emery-Dreifuss muscular dystrophy and Dunnigan-type lipodystrophy, respectively. Our structure determination and mutant analyses clearly show that the consequences of the mutations causing muscle-specific diseases or lipodystrophy are different at the molecular level.

Introduction

The eukaryotic nucleus is a complex organelle that contains the chromatin. It is the site of DNA replication, RNA transcription and processing, and ribosome assembly. These functions are highly dependent on the structural organization of the nucleus, which has to be dynamically rearranged during cell differentiation and cell cycle progression [1]. Two elements are important in establishing nuclear structure: (1) the nuclear membranes, which form the border between the nucleus and the cytoplasm and (2) the nuclear lamina, a meshwork of nuclear-specific intermediate filaments called lamins, associated with the inner nuclear membrane either directly or through interactions with membrane-bound proteins [2].

The nuclear lamina is essential for maintaining nuclear shape, spacing nuclear pore complexes, and anchoring and organizing heterochromatin [3]. During mitosis in higher eukaryotes, disassembly and reassembly of the nuclear lamina are required to complete the cell cycle [4, 5]. Cytological studies show that a large proportion of condensed chromatin borders the inner nuclear membrane, and that inner nuclear membrane proximity helps to repress partially silenced genes [6]. As many nuclear lamina proteins interact directly with chromosomal proteins, the lamina might also modulate the higher order structure of chromatin. Furthermore, the activities of several transcription factors including Rb, Oct1, Pdx1, and GCL involve interactions with the lamina, which suggests that the lamina plays an active role in transcriptional repression [7, 8]. Finally, during apoptosis, lamins are early targets for caspase degradation, and when their degradation is blocked, chromatin fails to condense and DNA cleavage is delayed (for a review, see [10]) [9]. Thus, lamin degradation facilitates nuclease activation during apoptosis.

Humans have three lamin genes [11]. The *LMNA* gene [12] encodes four alternatively spliced A-type lamins named A, C, $A_{\Delta 10}$, and C_2. Two genes encode B-type lamins, *LMNB1* (encoding lamin B1) and *LMNB2* (encoding lamins B2 and B3). A-type and B-type lamins are differentially expressed in cells. In general, lamin B2 is expressed at relatively constant levels throughout development. Lamin B1 is expressed mainly early in development and its expression correlates with proliferation. A-type lamins are expressed only during or after differentiation and their expression levels increase with terminal differentiation and growth arrest. A-type and B-type lamins also differ by their behavior and spatial distribution during mitosis, with A-type lamins being soluble and dispersed throughout the cytoplasm, whereas most B-type lamins remain associated with membranes.

All lamins are structurally type V intermediate filament

[6]Correspondence: szinn@cea.fr

Key words: dystrophy; Ig fold; lamin; laminopathies; nuclear lamina; NMR

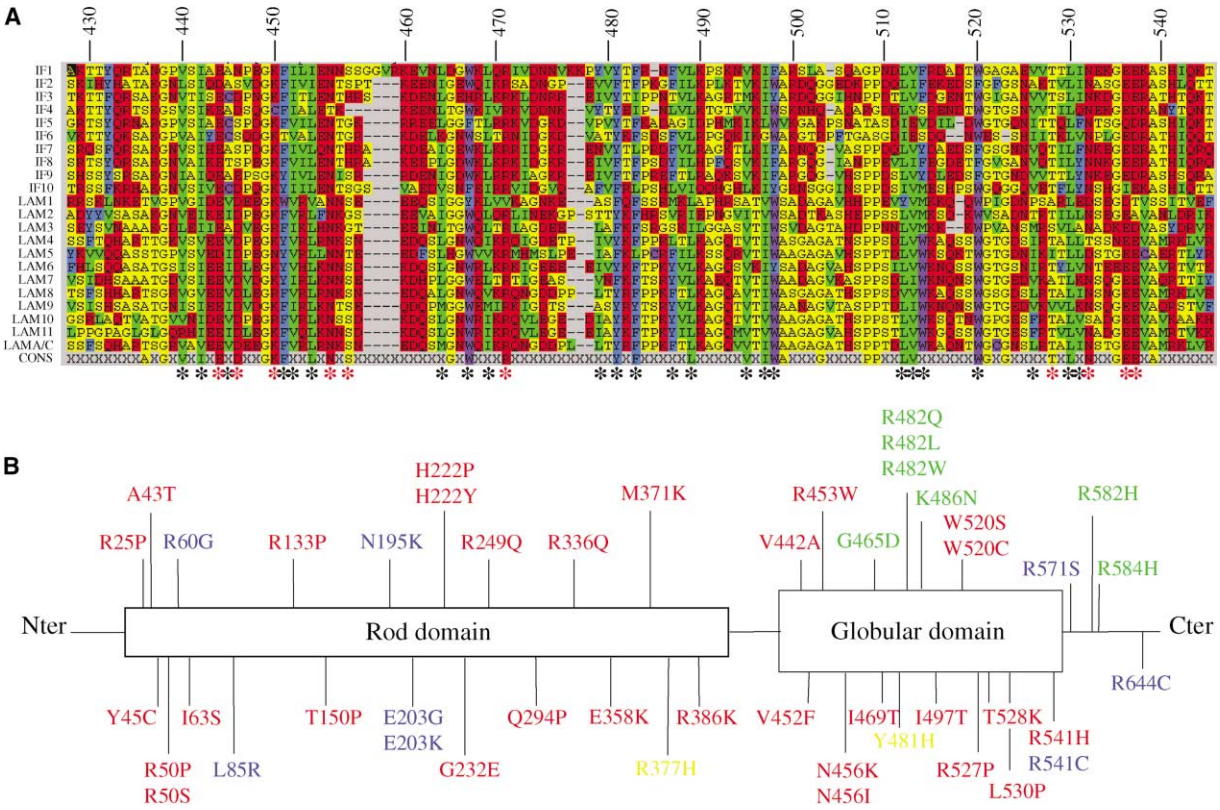

Figure 1. Analysis of the Primary Structure of Human Lamin A/C

(A) Multiple alignment of the C-terminal domain of the cytoplasmic invertebrate intermediate filaments (IF1 to IF10), invertebrate lamins (LAM1 to LAM3), and vertebrate lamins (LAM4 to LAMA/C), as obtained using Seaview. W residues are colored in purple, F and Y in blue, L, V, I, and M in green, and D, E, Q, N, K, and R in red; all other residues are colored in yellow. The selected sequences correspond to a highly divergent set extracted from the ensemble of sequences analogous to the C-terminal domain of human lamin A/C, as given by the Psi-Blast program [44, 51]. IF1 to IF10 refer to *H. aspersa* 70 kDa neurofilament protein (GenBank identifier 773571), *A. lumbricoides* cytoplasmic intermediate filament protein D1 (gi 784942), *A. suum* intermediate filament protein B (gi 124235), *L. pealei* 70 kDa neurofilament protein (gi 266617), *H. marmorata* filarin (gi 726492), *L. terrestris* intermediate filament protein (gi 633240), and *C. elegans* cytoplasmic intermediate filaments 1 (gi 1848063), 2 (gi 2198433), 4 (gi 1848062), and hypothetical protein F10C1.7a (gi 1203948), respectively. LAM1 to LAMA/C refer to *C. elegans* lamin (gi 450496), *D. melanogaster* lamin DM0 (gi 1346410), lamin C (gi 729915), *X. laevis* lamin A (gi 125963), lamin B3 (gi 125959), lamin B2 (gi 125958), lamin B1 (gi 125955), *G. gallus* lamin A (gi 125961), lamin B1 (gi 125952), *M. musculus* lamin B2 (gi 125957), *H. sapiens* lamin B2 (gi 8928567), and lamin A/C (gi 125962), respectively. The last line corresponds to a consensus sequence calculated above 60% of identity. It shows that 28% of the residues are conserved in this protein family. Black stars indicate hydrophobic residues of human lamin A/C which correspond to hydrophobic positions in more than 60% of the sequences. Red stars mark the conserved and polar residues. (B) Schematic map of the sequence localization of the missense mutations linked to the different laminopathies in human lamin A. Mutations causing Emery-Dreifuss muscular dystrophy are marked in red characters, limb girdle muscular dystrophy type 1B in yellow characters, dilated cardiomyopathy in blue characters, and Dunnigan-type familial partial lipodystrophy in green characters [17, 24].

proteins. From their sequences, it can be deduced that each lamin consists of a small N-terminal segment of about 30 residues, followed by a large α-helical rod domain of about 40 kDa and a C-terminal tail of about 20 kDa [13]. In the transmission electron microscope, lamin molecules appear as parallel, unstaggered dimers. A 16 amino acid segment at the rod domain N-terminal end and a 30 amino acid segment at the rod domain C-terminal end are highly conserved among lamins and play a crucial role in the association of lamin dimers into distinct higher order assemblies such as head-to-tail polymers. The final organization of lamin polymers within the 10 nm filaments is not known [3]. From an evolutionary point of view, the primary structure of lamins is more closely related to the cytoplasmic invertebrate intermediate filament proteins than to the vertebrate intermediate filament proteins [14]. The sequence conservation between lamins and invertebrate intermediate filament proteins is illustrated in Figure 1A.

The functional importance of the nuclear lamina has been emphasized recently by the discovery of human diseases caused by mutations in lamins or lamin-associated proteins. The X-linked form of Emery-Dreifuss muscular dystrophy (EDMD) is caused by mutations in the lamin-associated protein emerin [15], whereas autosomal dominant EDMD is caused by mutations in the *LMNA* gene that encodes lamins A and C [16]. Other mutations in *LMNA* cause limb girdle muscular dystrophy type 1B, dilated cardiomyopathy with conduction defects, and Dunnigan-type partial lipodystrophy (for a review, see [17]). The molecular mechanisms of these diseases, which are collectively called laminopathies, remain obscure [18]. Forty missense mutations causing muscle diseases have been identified so far. They are

spread out in the entire lamin molecule (Figure 1B). Mutations in the rod domain are generally predicted to modify the oligomerization state of the proteins, but how this results in muscle-specific disease is not clear. Seven missense mutations causing Dunnigan-type partial lipodystrophy are known. They are all located in the C-terminal tail (Figure 1B). The structural and functional consequences of mutations in this C-terminal tail are completely unknown. In particular, the variety of diseases caused by mutations of residues sequentially close is not explained.

In this paper, we present the three-dimensional solution structure of the C-terminal globular domain of human lamins A and C (lamin A/C) together with structural and thermostability data for three "hot spot" mutants. The structure determination and mutant analyses clearly show that mutations causing muscle-specific diseases are found at positions playing a critical structural role, whereas mutations causing Dunnigan-type lipodystrophy lead to a diminution of the positively charged character of a specific solvent-accessible region.

Results

Identification of the C-Terminal Globular Domain

The globular morphology of the C-terminal tail of lamin A/C has been previously revealed by electron microscopy (reviewed in [3]). Analysis of the lamin sequences using the HCA program [19, 20] and comparison between the lamin and invertebrate filament protein sequences (Figure 1A) strongly suggested that the C-terminal tail of all these proteins contains a conserved and folded domain. We chose to study the region between residues 411 and 553 of human lamin A/C, which includes this domain.

Is the C-Terminal Domain of Lamin A/C Monomeric in Solution?

Analytic ultracentrifugation was used in order to characterize the oligomerization state of lamin A/C C-terminal domain. In a phosphate buffer at pH 6.3 and in the presence of DTT, the lamin A/C C-terminal domain was observed essentially in a monomeric state. This indicates that the protein does not self-associate at a concentration lower than 50 μM.

Solution Structure Determination

We have solved the structure of the C-terminal domain of lamin A/C using heteronuclear double and triple resonance NMR spectroscopy. Assignment of ^{1}H, ^{15}N, and ^{13}C chemical shifts was achieved at 30°C and pH 6.3 between Ser 428 and Val 547. The segments 411–427 and 548–553 are unstructured.

The solution structure of the region 428–547 was solved on the basis of the analysis of 1637 nOe cross-peaks (993 and 644 were picked on the ^{15}N-HSQC-NOESY and ^{13}C-HSQC-NOESY, respectively). At the end of the assignment and structure calculation procedure, 89 peaks remained unassigned. On the basis of the 1548 other peaks, 1401 restraints were generated. Forty restraints were not used in the calculations because they led to systematic violations higher than 0.5 Å. The structure was calculated on the basis of the 1361 remaining distance restraints. Thus, the mean number of distance restraints per residue yields 11.7 between Phe 430 and Arg 545. Furthermore, 19 ϕ torsion angle values were deduced from the analysis of the HN-HA experiment, and 64 couples of (ϕ,Ψ) torsion angles were derived from backbone ^{1}H, ^{15}N, and ^{13}C chemical shifts using the program TALOS [21]. Finally, 36 hydrogen bonds were constrained in the β structure, when H-D exchange experiments showed that the corresponding amide protons were protected against solvent exchange.

Table 1. Structural Statistics

Number of violations	
nOe distance restraints > 0.5 (Å)	0
Dihedral restraints > 10°	0
Rms deviation from experimental restraints	
nOe distance restraints (Å)	0.050 ± 0.002
Dihedral angle restraints (°)	0.66 ± 0.17
Rms deviation from idealized covalent geometry	
Bonds (Å)	0.0195 ± 0.0002
Angles (°)	3.48 ± 0.05
Improper (°)	0.051 ± 0.002
Energy[a]	
van der Waals (kcal/mol)	22.8 ± 15.0
Electrostatic (kcal/mol)	−671.5 ± 19.0
Ramachandran analysis	
Residues in most favored region (%)	74.0
Coordinate precision (residues 430–545)	
Backbone atoms (Å)	0.62 ± 0.14
All heavy atoms (Å)	1.26 ± 0.13

[a] The van der Waals energy is calculated with a Lennard-Jones potential. The electrostatic energy is calculated with no net charges on side chain atoms and a distance-gated dielectric constant. CHARMM22 parameters were used.

Analysis of the 15 final structures (Table 1) shows that no distance violations larger than 0.5 Å are present. Furthermore, the covalent geometry is respected, as evidenced by the low root-mean-square deviation (rmsd) value for bond lengths and valence angles. The value of the van der Waals energy is small, indicating that there are no incorrect nonbonded contacts.

Description of the Backbone Structure

The C-terminal domain of lamin A/C adopts an immunoglobulin (Ig) fold of type s. Its topology is described in Figure 2. It consists of nine β strands, forming two β sheets of four and five strands, respectively, packed into a classical β sandwich. Strands 1, 4, 5, 8, and 9 are involved in the first β sheet. Strands 2, 3, 6, and 7 form the second β sheet, β7 being parallel to β6. Strands 2, 3, 4, 5, 6, 8, and 9 compose the classical Ig fold of type s and correspond to strands A, B, C, C′, E, F, and G, respectively, following the Ig fold nomenclature. Strands 1 and 7 are additional strands typical of the lamin fold.

Figure 3 shows a stereo view of the final structures. The conformation of the backbone is well defined for residues 430–545. The rmsd for C, N, and Cα atoms with respect to the mean coordinates is close to 0.6 Å. The Ramachandran plot of the protein segment 430–545

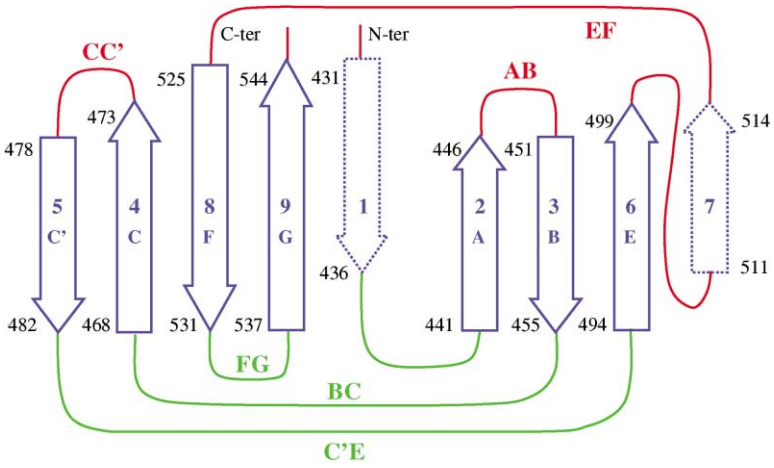

Figure 2. Topology of the Lamin A/C C-Terminal Domain

The β strands belonging to the two β sheets are displayed as blue arrows. Their limits are indicated next to the extremities of the arrows. Blue arrows correspond to the β strands forming the classical Ig fold of type s, whereas dotted blue arrows represent the additional β strands characteristic of the lamin fold. Loops located on the N-terminal side of the β sandwich are colored in red and loops located on the opposite side are colored in green.

confirms the good quality of the structures as no residues are systematically in the disallowed region. Over the 15 structures, the percentage of residues in the most favored and additional allowed region yields 96.8%.

The β sandwich of the lamin A/C domain is characterized by a large tilt of about 45 degrees between the axes of the two β sheet layers (Figures 2 and 3). These β sheets are mainly regular. They show two classic β bulges. Residues Arg 453 in β3 and Glu 443, Glu 444 in β2 form the first β bulge (consistently, the three amide protons are protected against exchange with solvent; Figure 4C). Ile 531 in β8 and Val 538, Ala 539 in β9 form the second β bulge (the amide protons of residues 531 and 538 are protected; Figure 4C). Both β bulges are probably present in all lamin homologs (Figure 1A).

Several loops are found at each extremity of the β sandwich (Figures 2 and 3). The N and C termini are located at one of these extremities, together with the 4 residue loop β2β3 (i.e., loop AB, following the Ig fold nomenclature), the 4 residue loop β4β5 (i.e., loop CC′), the 4 residue loop following β6, and the large loop β7β8 (both loops are comprised in the so-called loop EF of the classical Ig fold). At the other extremity, the 4 residue loop β1β2, the two large loops β3β4 (i.e., loop BC) and β5β6 (i.e., loop C′E), a small loop before β7, and the 5 residue loop β8β9 (i.e., loop FG) are observed. Both BC and C′E large loops contain a β strand at positions 458–463 and 487–491, respectively. These strands are involved in a small β sheet stabilized by three hydrogen bonds (462 HN-489 O, 464 HN-487 O, and 489 HN-462 O; the three corresponding amide protons are not completely exchanged after 48 hr in D_2O as shown in Figure 4C). At the end of loop β6β7, the motif Pro-Pro conserved in all lamins and in most of the invertebrate intermediate filaments (Figure 1A) is characterized by the presence of a *cis* peptide bond between Pro 508 and Pro 509. The 5 residue loop β8β9 (FG) contains a turn between Asn 532 and Gly 535. This turn has torsion angles and an i → i + 4 hydrogen bond typical of a type I β turn, except that residue i + 4 (Gly 535) adopts an α_L conformation. Loop β8β9 is also stabilized by hydrogen bonds between residues 532 and 536 (532 HN-536 O and 536 HN-532 OD_1; both amide protons are not exchanged after 48 hr as shown in Figure 4C). Finally, it must be stressed that the loops BC, C′E, and FG are well defined compared to the loops AB, CC′, and EF located on the other side of the β sandwich (Figure 3).

Identification of the Hydrophobic Core

In the C-terminal domain of lamin A/C, 24 hydrophobic residues correspond to conserved hydrophobic positions in more than 60% of a divergent subset of analogous sequences (Figure 1A). Analysis of these 24 hydrophobic residues shows that, in general, (1) their side

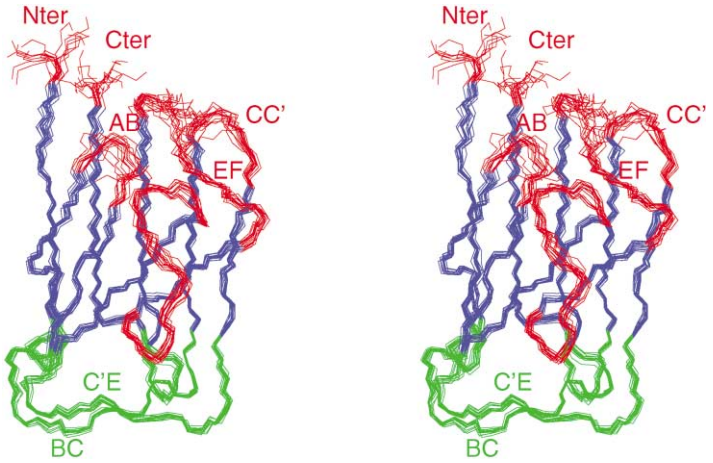

Figure 3. Superposition of 15 Three-Dimensional Backbone Structures (in Stereo) of the Human Lamin A/C C-Terminal Domain

β strands are displayed in blue, and loops in red and green as in Figure 2.

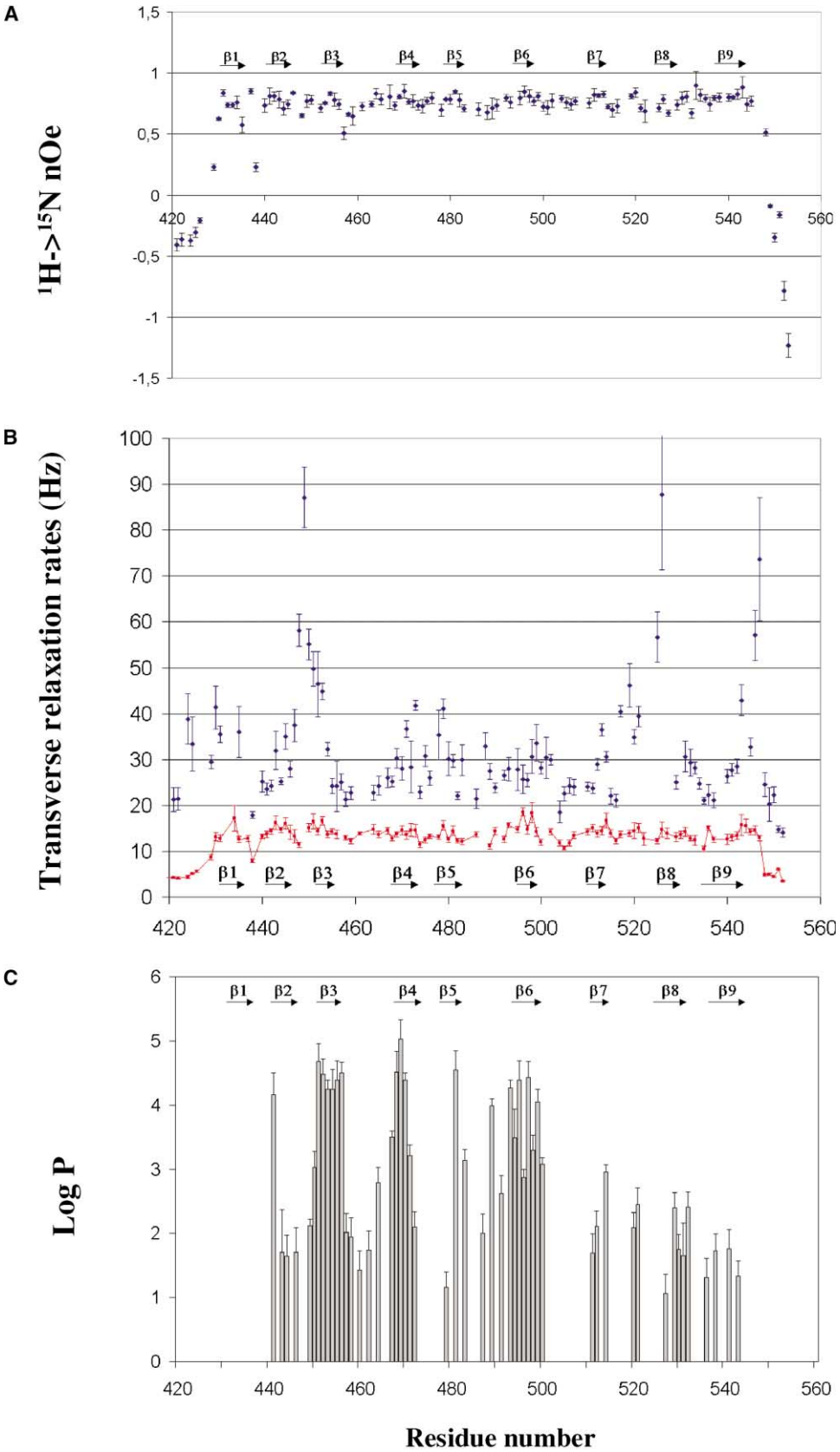

Figure 4. Parameters Characterizing the Dynamics Behavior of the C-Terminal Domain of Lamin A/C

^{1}H→^{15}N nOe values (A), ^{15}N $R_{1\rho}$ (red marks) and R_2 values (blue marks) (B), and protection factors against solvent exchange of the amide protons (C) are displayed as a function of residue number.

chains are less than 20% solvent accessible and (2) they belong to (or are next to) the β structure. Thus, they are mainly involved in the core of the molecule. In particular, in order to stabilize the β sandwich, Val 440, Val 442, and Val 445 from (or next to) β2 strand, Val 452, Leu 454 from β3 strand, Val 495, Ile 497 from β6 strand, and Leu 512, Trp 514 from β7 strand are packed against Trp 467, Ile 469, from (or next to) β4 strand, Leu 479, Tyr 481, Phe 483 from (or next to) β5 strand, and Leu 526, Leu 530 from β8 strand (see Figures 1A and 2). At one extremity of the β sandwich, Met 464, Trp 467 in loop BC and Phe 487, Leu 489 in loop C′E are in contact with residues of the two main β sheets. They participate in the stabilization of the β sandwich and in the positioning of loops BC and C′E relative to the β structure (Figures 2 and 3). In contrast, at the other extremity of the β sandwich, the large loop β7β8 contains a unique hydrophobic residue, Trp 520. This residue is close to Trp 498 (β6) and Trp 514 (β7), suggesting that it is involved in the structuring and the positioning of loop β7β8. However, its solvent accessibility varies within our 15 structures, as the conformation of loop β7β8 is ill defined.

Role of the Conserved and Buried Polar Residues

Ten polar residues are conserved within the set of sequences homologous to the C-terminal domain of lamin A/C (Figure 1A). Within these residues, Asn 456, Arg 471, Thr 528, and Asn 532 show extremely buried side chains (i.e., their side chain solvent accessibility is lower than 20%). Asn 456, next to β3 strand, makes hydrogen bonds throughout its side chain amide protons with the backbone oxygens of Glu 460 and Leu 489, located in loops BC and C′E, respectively. The presence of these hydrogen bonds is consistent with the experimentally observed strong protection of the Asn 456 side chain amide protons against exchange with water. Arg 471 (β4) and Thr 528 (β8) point toward the core of the β sandwich, their side chains making hydrogen bonds with different backbone or side chain oxygens depending on the structures. Finally, Asn 532 makes a hydrogen bond throughout its side chain with Glu 536 amide proton in the type I β turn 532–535 of loop β8β9, and the amide proton of residue 536 is consistently protected against solvent exchange.

Structure Dynamics

^{15}N R_1, $R_{1\rho}$, and R_2 relaxation rates and $^1H \rightarrow ^{15}N$ nuclear Overhauser effects (nOe) were measured in order to investigate the motions of the lamin A/C C-terminal domain. Figure 4A shows the values of the $^1H \rightarrow ^{15}N$ nOe, which is essentially sensitive to rapid (i.e., picosecond to nanosecond time scale) motions, as a function of residue number. A value close to 0.83, characteristic of highly restricted rapid motions, is found for most of the residues belonging to the β strands. Lower values between 0.6 and 0.7 are observed in the loops. Negative values correspond to completely unstructured segments. Clearly, only the region between Phe 430 and Arg 545 of the 411–553 polypeptide adopts a stable conformation on the picosecond to nanosecond time scale. This result is consistent with the high resolution of the solution structures between Phe 430 and Arg 545.

^{15}N $R_{1\rho}$ and R_2 values were compared in order to identify protein regions involved in slower motions (Figure 4B). Large differences between the two parameters reflect the existence of millisecond time scale motions. Interestingly, these motions are present on the whole structure. The R_2-$R_{1\rho}$ value is particularly large for residues located around the solvent-exposed Cys 522, that is, for the first residues of strand β1, the loops β2β3 (AB), the end of loop β7β8 (EF), the first 2 residues of β8, and the 2 residues following β9 at the C terminus (Figures 2 and 4B). Thus, residues located around Cys 522 exhibit particularly large or slow chemical environment variations on a millisecond time scale. Consistently, only 22% of the amide protons are protected from solvent exchange in the loops AB, CC′, and EF close to Cys 522, whereas 50% of the amide protons are protected from solvent exchange within loops BC, C′E, and FG (Figure 4C). Interestingly, the most flexible loop region on a millisecond time scale is also the less well-defined region of the structure (Figure 3). Finally, analysis of the ^{15}N R_1, $R_{1\rho}$, and $^1H \rightarrow ^{15}N$ nOe values shows that the global rotational correlation time of the molecule is about 10 ns, which confirms that the lamin A/C C-terminal domain essentially behaves as a monomer in solution.

Where Are the Different Mutations of the Lamin A/C C-Terminal Domain Linked to the Different Pathologies?

The C-terminal domain of lamin A/C is mutated in four heritable diseases (Figure 1B). Three of them, Emery-Dreifuss muscular dystrophy, limb girdle muscular dystrophy type 1B, and dilated cardiomyopathy, are characterized by cardiac abnormalities, and, in the case of the two muscular dystrophies, progressive skeletal muscle wasting. The fourth disease, Dunnigan-type familial partial lipodystrophy, is characterized by regional fat loss, insulin resistance, and diabetes mellitus with no striated muscle abnormalities.

Mutations throughout the lamin A/C protein have been identified in patients with Emery-Dreifuss muscular dystrophy. Thirteen of the missense mutations are in the C-terminal domain. These are V442A, V452F, R453W, N456K and N456I, I469T, I497T, W520S and W520C, R527P, T528K, L530P and R541H (Figure 1B and our unpublished data) [22–24]. Apart from R453W and R527P, all the mutations concern buried residues localized in the core of the 3D structure (Figure 5A). Among them, V442A, V452F, I469T, I497T, and L530P correspond to hydrophobic residues of the β sheet and W520S, W520C correspond to the unique hydrophobic residue of the EF loop. The hydrophobic character of these residues is conserved in most lamin homologs (Figure 1A). N456K, N456I, and T528K mutations correspond to buried polar residues also conserved in most lamin homologs (Figure 1A). Their side chains are involved in hydrogen bonds that stabilize the conformation of the loops BC and C′E in the case of Asn 456 and the β sandwich in the case of Thr 528. Finally, the buried side chain of Arg 541 participates in the stabilization of the β sandwich through hydrophobic contacts with the core of the domain. Such interactions are disrupted by

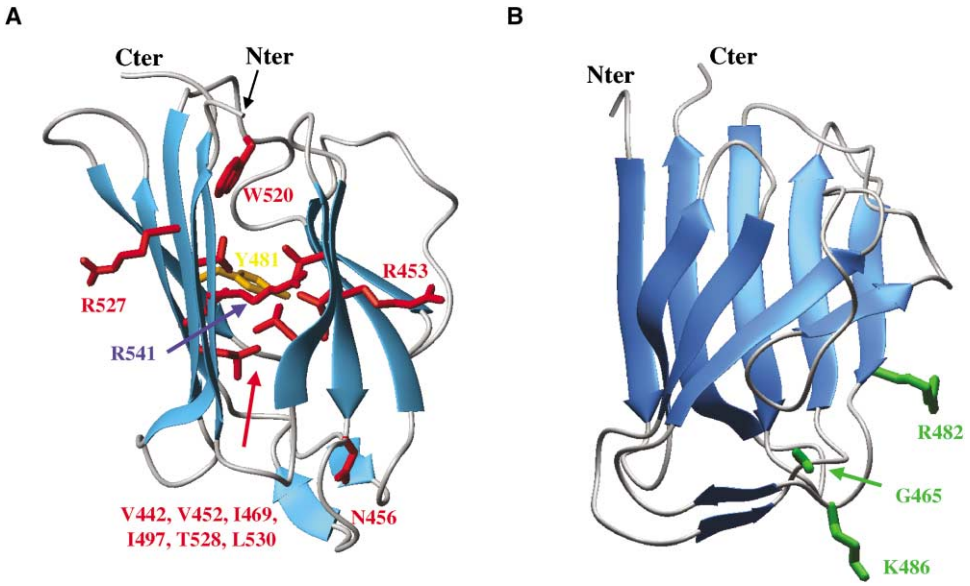

Figure 5. Localization in the Ig-like Structure of the Mutations Associated with Heritable Diseases

(A) Localization of the mutations causing diseases characterized by cardiac and skeletal muscle abnormalities.

(B) Localization of the mutations causing Dunnigan-type familial partial lipodystrophy.

Orientation of the domain in (B) is the same as that in Figure 3, while a rotation of 90° around the vertical axis gives the orientation of the domain in (A). Mutated residues are colored as in Figure 1B; mutations causing Emery-Dreifuss muscular dystrophy are in red, limb girdle muscular dystrophy type 1B in yellow, and Dunnigan-type familial partial lipodystrophy in green. The Arg 541 residue is mutated in two diseases: Emery-Dreifuss muscular dystrophy (R541H) and dilated cardiomyopathy with conduction defects (R541C).

its mutation to histidine. Two solvent-exposed arginines are also mutated in patients with Emery-Dreifuss muscular dystrophy. Arg 453 is at the center of a β sheet. It is involved in a salt bridge with Glu 444. This salt bridge is conserved in lamins (Figure 1A) and is disrupted by the mutation of Arg 453 to tryptophan. Arg 527 is located at the center of the other β sheet. Thus, its amide proton is involved in a backbone-backbone hydrogen bond (it is consistently protected against solvent exchange). Mutation of Arg 527 to proline disrupts the β sheet hydrogen bond network. From this analysis, we conclude that mutations that cause Emery-Dreifuss muscular dystrophy probably destabilize the three-dimensional structure of the C-terminal domain of lamin A/C.

Only one missense mutation of the C-terminal domain of lamin A/C has been shown to cause limb girdle muscular dystrophy of type 1B (Figure 5A) [25]. It is Y481H, which corresponds to the replacement of a conserved residue of the hydrophobic core by a polar residue. This again should lead to a destabilization of the domain structure. One mutation in the Ig-like domain, R541C, causes dilated cardiomyopathy (Figure 5A; G.B., unpublished data). It corresponds to the replacement of a buried arginine by a cysteine and should also lead to a destabilization of the domain structure.

Virtually all the mutations that cause Dunnigan-type familial partial lipodystrophy are found in the C-terminal tail of lamin A/C (Figure 1B) [26–29]. Five of these (G465D, R482Q, R482W, R482L, and K486N) are located in the Ig-like domain. Interestingly, the 3 mutated residues are close in the three-dimensional structure of the domain as shown in Figure 5B. Arg 482 and Lys 486 are largely solvent exposed. Positively charged residues are found at these two positions in most vertebrate lamins (Figure 1A). Gly 465 is also largely conserved in most lamin homologs (Figure 1A). The five mutations lead either to the suppression of a positive charge or to the appearance of a negative charge. Thus, Dunnigan-type familial partial lipodystrophy is linked to a diminution of the positively charged character, conserved in vertebrate lamins, of a site defined by the 3 mutated residues. Interestingly, this site is located in a large solvent-exposed surface which presents no negative charge in the native human lamin A/C (Figure 6A). Finally, a patient severely affected by Dunnigan-type lipodystrophy was found as a heterozygote for both V440M and R482Q [30]. However, the mutation V440M seems not to cause lipodystrophy on its own. Interestingly, this observation is consistent with our analysis, as Val 440 belongs to the hydrophobic core of the C-terminal domain and not to the positively charged patch described above, whereas Arg 482 is part of the solvent-exposed and positively charged patch.

Structural Analysis of Three Hot Spot Mutants, R453W, R482W, and R482Q

In order to validate our structural analysis, we have characterized the structure and thermostability of three hot spot mutants using NMR and circular dichroism. The chosen mutants are particularly representative: R453W and R482Q/L/W occur in 14% and 12% of the patients affected by a laminopathy, respectively. Furthermore, R482Q/L/W mutations are found in 90% of the patients with a Dunnigan-type familial partial lipodystrophy. Figure 7 illustrates the consequences of the mutations R453W, R482W, and R482Q on the lamin C-terminal

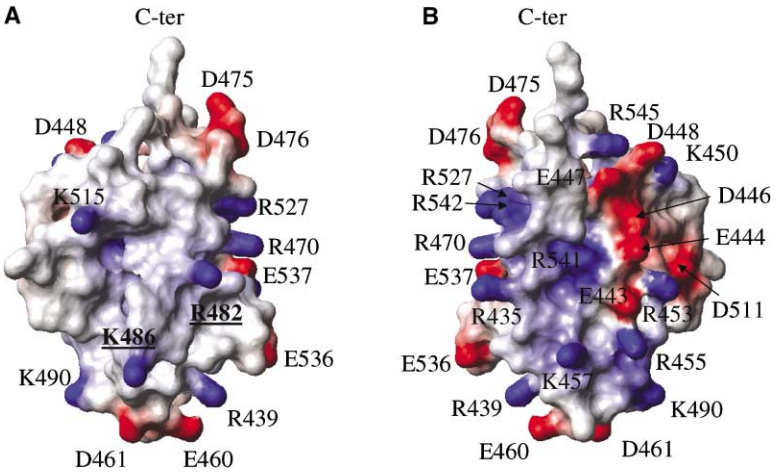

Figure 6. Face and Back Views of the Electrostatic Potential at the Surface of the C-Terminal Domain of Human Lamin A/C

Calculated by MOLMOL [48]. The surface comprising the charged residues Arg 482 and Lys 486 mutated in Dunnigan-type familial partial lipodystrophy is shown in (A). The orientation of the domain in (A) corresponds to that of Figure 5B rotated by 90° around the vertical axis. The orientation of the domain in (B) corresponds to that of Figure 5A.

domain mean structure and stability. The CD spectrum of the wild-type domain is typical of a β sheet structure (Figure 7A). The evolution of this spectrum as a function of temperature shows that the denaturation temperature of the wild-type domain is 62°C (Figures 7A and 7B). Similar CD spectra and denaturation temperatures are found for the mutants R482W and R482Q (Figure 7B). The CD spectrum of the R453W mutant is also similar to that of the wild-type domain at 10°C. However, the denaturation temperature of this mutant is only 43°C, and at 37°C a significant population of this mutant is already unfolded (Figure 7B). Thus, the mean structures of the three mutants are close to the native β structure at 10°C and the mutations R482W and R482Q do not destabilize this structure. In contrast, the mutation R453W strongly destabilizes the lamin C-terminal domain structure. Another experimental method was used to confirm these results. As shown in Figure 7C, the ^{1}H NMR spectra of the mutants R482W and R482Q are similar to the spectrum of the native domain, showing that these mutations have no impact on the solution structure of the domain. In contrast, the NMR spectrum of the R453W mutant shows much larger line widths than that of the native domain spectrum, and several proton resonances have shifted toward frequencies characteristic of random structure. These data indicate that the R453W mutant exhibits very large motions on a millisecond time scale around its mean structure, which confirms that the structure of the lamin C-terminal domain is strongly destabilized by this mutation.

Discussion

Presentation of the Three-Dimensional Structure of Lamin A/C

We have demonstrated here the presence of an immunoglobulin-like domain in the tail region of cytoplasmic invertebrate intermediate filaments and nuclear lamins. In human lamin A/C, this domain consists of 116 residues folded into a β sandwich of nine β strands (Figures 2 and 3). Seven of these strands are present in the classical Ig fold topology. Strands 1 and 7 are additional strands typical of the lamin fold (Figure 2).

Dynamics of the C-Terminal Domain of Lamin A/C

Ultracentrifugation and NMR relaxation experiments showed that the lamin A/C C-terminal domain is mainly monomeric under our experimental conditions. However, the structure fluctuates between different conformations on a millisecond time scale. As these fluctuations implicate the whole lamin domain, they are probably due to a breathing of the β structure in solution, characterized in particular by different possible positioning of the aromatic residues. Such global motion has already been described for the third fibronectin type III domain of human tenascin-C [31]. Interestingly, both lamin and tenascin domains were isolated from a larger protein, adopt an Ig-like fold, and participate in a large number of distinct interactions in the cell. These domains share a conformational energy landscape consistent with large millisecond time scale motions. Their flexibility might result from the absence of the other protein domains. It might also be a property of the native domains, which is important for their adaptability to various biological partners.

It must be stressed that in the case of the lamin Ig-like domain, particularly large chemical environment fluctuations are detected around the solvent-exposed Cys 522. This could be due to a dimerization of the protein through the formation of a transient disulfide bridge arising on a millisecond time scale, even if the population of dimers is small compared to the population of monomers under our conditions.

Is It Possible to Predict the Ig Fold of the Lamin A/C C-Terminal Domain?

The Ig fold is one of the most common protein folds. It occurs in many proteins having no detectable sequence similarity, and no sequence signature exists for this fold [32, 33]. In the case of the C-terminal domain of lamin A/C, less than 20% of identity is found with proteins known to adopt an Ig fold. Threading programs such as 3D-PSSM [34] propose the Ig fold as a possible fold for the lamin C-terminal domain within several other folds but no such program could predict with certainty the structural family to which the lamin C-terminal domain

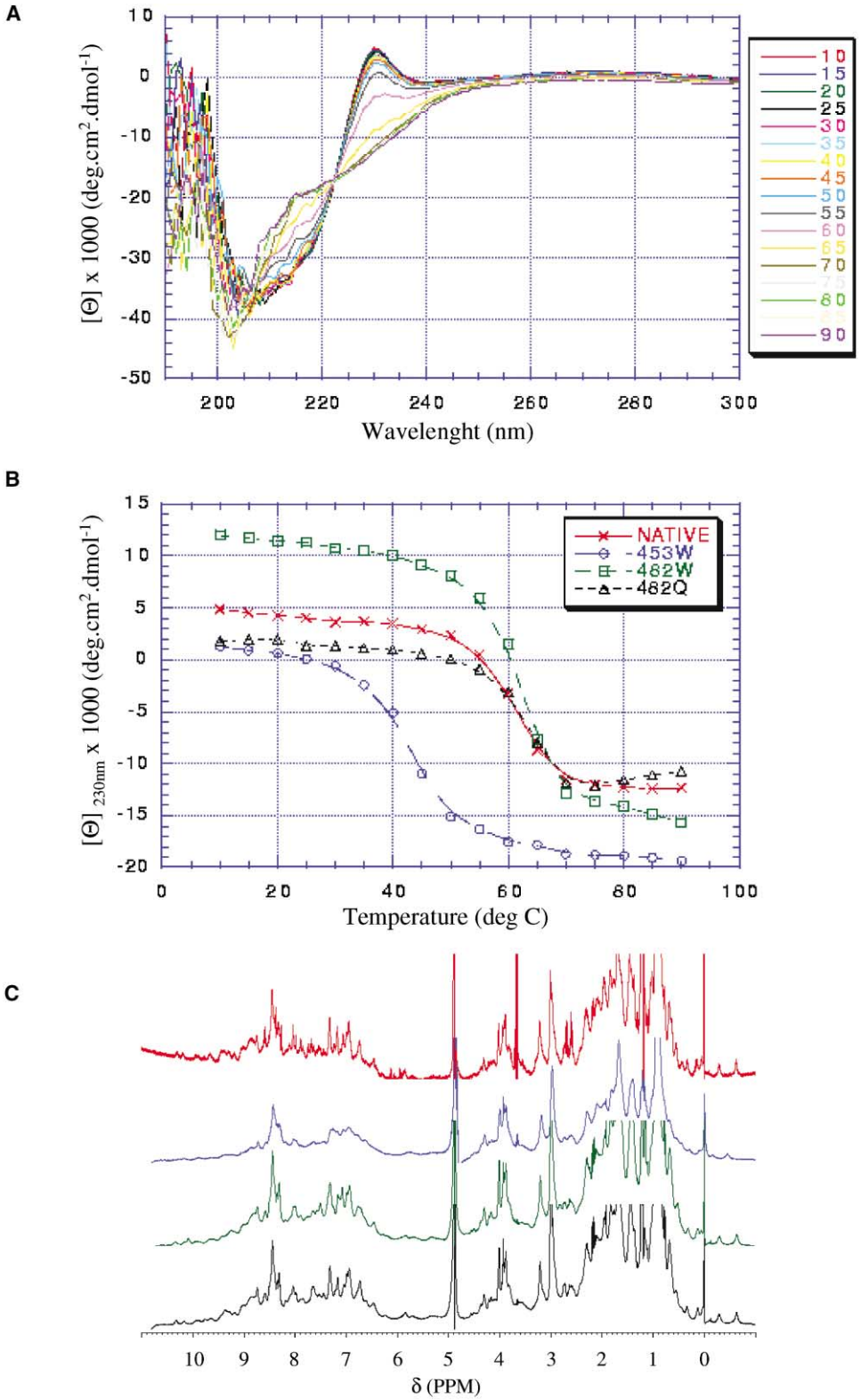

Figure 7. Structural Characterization of Three Mutants, R453W, R482W, and R482Q, by Circular Dichroism (CD) and NMR

(A) Evolution of the CD spectrum of the wild-type Ig-like domain as a function of temperature. Curves corresponding to temperatures from 10 to 90°C are displayed according to the boxed color code at the right of the diagram.

(B) Molar residual ellipticity measured at 230 nm as a function of the temperature for the wild-type domain and the three mutants.

(C) Proton 1D NMR spectra of the wild-type domain and the three mutants recorded at 20°C and plotted using the same color code as in (B).

belongs. Analysis of a representative set of sequences of Ig-like proteins from the Protein Data Bank [35] using the HCA program [19, 20] showed that the analogy between the C-terminal domain of lamin and several Ig-like proteins, concentrated on strands A, B, C, C′, E, F, and G, is assessed by significant Z scores for identity, similarity (using BLOSUM62 matrix), and hydrophobic matching. For example, when comparing our domain to the VL domain of the antibody corresponding to the Protein Data Bank code 1UCB, the ratio between the product of these three indices and the best product calculated from 1000 randomized sequences at constant amino acid composition yields 10. Although weak, there is therefore a primary structure memory between lamin A/C and Ig fold proteins, which appears clearly when the structural alignment is known. At the three-dimensional structure level, superposition of the lamin C-terminal domain with the VL domain of 1UCB for 75% of the residues of the seven common strands shows that the backbone root-mean-square deviation is as small as 1.8 Å. A reasonable model of most of the β sandwich of the lamin A/C C-terminal domain could thus be constructed knowing how to align the sequences of 1UCB and lamin A/C.

Differential Localization of the Mutations Linked to Laminopathies

Mutations causing Emery-Dreifuss muscular dystrophy, limb girdle muscular dystrophy type 1B, and dilated cardiomyopathy are found at positions playing a critical structural role in the C-terminal domain of lamin A/C. These positions essentially correspond to conserved hydrophobic residues and buried conserved polar residues (Figures 1A and 5A). In contrast, mutations causing Dunnigan-type familial partial lipodystrophy correspond to three positions close in space and solvent accessible (Figure 5B). These mutations lead to a diminution of the conserved positively charged character of a site defined by the 3 mutated residues (Figure 6). Thus, the structure determination of the C-terminal domain of human lamin A/C strongly suggests that the mutations causing muscle-specific diseases destabilize the lamin Ig-like domain, while the mutations associated with lipodystrophy do not affect the 3D structure but destroy a positively charged interaction site of lamin A/C for a yet unidentified specific class of biological partners. These suggestions are supported by the characterization of the consequences of three representative mutations, R453W (EDMD) and R482W/Q (lipodystrophy), on the structure and thermostability of the domain. Whereas the mean structures of the three mutants are similar to the structure of the wild-type domain at 10°C, the R453W mutation is characterized by a 20°C loss of denaturation temperature as compared to the wild-type and the R482W/Q mutants.

Emery-Dreifuss muscular dystrophy, limb girdle muscular dystrophy type 1B, and dilated cardiomyopathy are also linked to mutations in the rod domain of lamin A/C. The common effect of mutations linked to these pathologies could be a destabilization of the whole lamin A/C molecule and likely of the lamin nuclear filaments. Such a dramatic influence on the lamin structure should lead to a global loss of function of the type A lamins. In the case of Dunnigan-type familial partial lipodystrophy, mutations are found in a specific solvent-exposed and positively charged region of the C-terminal domain (at positions 465, 482, and 486) and in a 3 residue segment of the disordered C-terminal tail (at positions 582 and 584; see Figure 1B). All these mutations lead to a diminution of the positively charged character of the affected regions. They could perturb the interaction of lamins with a specific class of biological partners, such as a protein family of the inner nuclear membrane or DNA, thus leading to a specific gain of function.

Which Are the Targets for the C-Terminal Domain of Lamin A/C?

The binding features of Ig-like domains are extremely diverse [32]. In the case of lamin A/C, it is known that a domain extending between residues 319 and 572, containing the Ig-like domain, binds to the α-specific region of lamina-associated protein 2α (LAP2α) [36]. LAP2α is a soluble protein implicated in nuclear structure organization during the cell cycle. Furthermore, region 384–566 of lamin A/C, which also contains the Ig-like domain, binds to the inner nuclear membrane protein emerin [37]. It must be stressed that a recent publication indicates that the R482Q lamin mutation has no influence on lamin-emerin interaction [38]. Thus, emerin probably does not interact with lamin A/C through the positively charged patch affected in Dunnigan-type lipodystrophy. Finally, lamin A/C has been shown to bind to DNA (for a review, see [3]). Thus, the lamin Ig-like domain could be involved both in protein and DNA binding.

Biological Implications

Lamins are nuclear intermediate filaments that together with lamin-associated proteins maintain nuclear shape and provide a structural support for chromosomes and replicating DNA. We have determined the solution structure of the C-terminal globular domain of human type A lamins. This domain encompasses residues 430–545 and adopts an Ig-like fold of type s. It is mutated in four heritable diseases. Three of them, Emery-Dreifuss muscular dystrophy, limb girdle muscular dystrophy type 1B, and dilated cardiomyopathy, are characterized by cardiac abnormalities, and, in the case of the two muscular dystrophies, progressive skeletal muscle wasting. The fourth disease, Dunnigan-type familial partial lipodystrophy, is characterized by regional fat loss, insulin resistance, and diabetes mellitus with no striated muscle abnormalities.

Analysis of the 3D solution structure of the C-terminal domain of human type A lamins and structural characterization of three "hot spot" mutants corresponding to Emery-Dreifuss muscular dystrophy and Dunnigan-type partial familial lipodystrophy, respectively, have shed some light on the molecular mechanisms involved in the different laminopathies. A model for these diseases is proposed in which mutations causing Dunnigan-type familial partial lipodystrophy do not alter the 3D structure but destroy the binding site for a class of lamin A/C biological targets, thus leading to a specific gain of func-

tion of type A lamins. In contrast, destabilization of the whole lamin protein by mutations causing Emery-Dreifuss muscular dystrophy, limb girdle muscular dystrophy type 1B, and dilated cardiomyopathy perturb the structure of the lamin nuclear filaments, thus leading to a global loss of function of the type A lamins. It is still far from clear how the different mutations eventually give rise to muscle-specific diseases or lipodystrophies. However, the consequences of the mutations in lamin A/C can be amplified by the fact that loss of specific attachment sites on the nuclear lamina, needed to establish or maintain particular patterns of gene expression, can result in defects in tissue-specific gene expression [2]. It is already known that lamins colocalize with transcriptional repressors such as the retinoblastoma protein [7]. Discovery of new partners for lamin proteins, and in particular of molecules targeting the positively charged patch affected by Dunnigan-type familial partial lipodystrophy, is now needed for a further understanding of the mechanisms perturbed in the different laminopathies.

Experimental Procedures

Sample Preparation

All cloning procedures were performed according to standard methods [39]. cDNA encoding amino acids 411–553 of lamins A and C was generated by polymerase chain reaction with a thermostable DNA polymerase [40] using the Gene Amp PCR System 2400 (Applied Biosystems). A BamHI restriction site was engineered at the 5′ end of the sense primer and an EcoRI restriction site at the 5′ end of the antisense primer, with lamin A cDNA [41] used as a template. The PCR product was digested with these restriction endonucleases and ligated into plasmid pGEX-4T-1 (Amersham Pharmacia Biotech). pGEX-4T-1 encodes glutathione-S-transferase (GST) and a thrombin cleavage site 5′ to the multiple cloning site. The resulting plasmid was transformed into *Escherichia coli* strain BL21. Expression and purification of the GST-lamin fusion protein was according to the manufacturer's instructions, using glutathione Sepharose 4B (Amersham Pharmacia Biotech). Purified chimeric protein was digested with thrombin protease, cleaving the lamin fragment from GST.

Labeled protein was obtained by growing recombinant strain in different labeled media. Uniformly labeled ^{15}N protein was produced in minimum media M9 containing 0.7 g/L of $(^{15}NH_4)_2SO_4$ (Boehringer). Uniformly labeled $^{13}C/^{15}N$ protein was produced in a rich labeled medium prepared from uniformly labeled $^{13}C/^{15}N$ *Spirulina maxima* cyanobacteria. For the analytic ultracentrifugation and circular dichroism experiments, protein concentration was between 10 and 50 μM. The solvent was a buffer of 20 mM sodium phosphate (pH 6.3) containing 0.1 mM DTT. For the NMR experiments, samples contained 0.1–1 mM protein dissolved in 20 mM phosphate buffer (pH 6.3) containing 2 mM DTT, 1 mM EDTA, and 0.1 mM NaN_3. 3-(trimethylsilyl)[2,2,3,3-$^2H_4$]propionate was added as a chemical shift reference.

Analytic Ultracentrifugation Experiments

Sedimentation equilibrium was performed at 30°C on a Beckman Optima XLA ultracentrifuge using an AN 60 Ti rotor and cells with a 12 mm optical path length. Sample volumes of 100 μl were centrifuged at 30,000 and 40,000 rpm. Radial scans of absorbance at 274 nm were taken at 3 hr intervals and equilibrium was achieved after 60 hr. Data were analyzed using the XL-A/XL-2 software supplied by Beckman.

NMR Spectroscopy

All experiments were performed at 30°C on Bruker DRX-500, DRX-600, or DRX-800 spectrometers, except the 1D experiments shown in Figure 7, which were carried out at 20°C on a Bruker DRX-500 spectrometer. Spectra were processed with the programs Xwinnmr (Bruker) and NMRPipe [42], and were analyzed using Felix (Molecular Simulations). Sequential assignment of ^1H, ^{15}N, and ^{13}C resonances was achieved by means of through-bond heteronuclear scalar correlations along the protein backbone and side chains [43, 44] using 3D HNHA, HNCO, HNCA, HN(CO)CA, CBCACONH, HBHACONH, HNCACB, HCCH-TOCSY, and with ^{13}C-HSQC NOESY experiments. Interproton distance restraints were derived from 3D ^{15}N- and ^{13}C- edited HSQC NOESY experiments, recorded at 800 MHz using a 150 ms mixing time. $^3J_{HNH\alpha}$ coupling constants were estimated from an HNHA experiment. In order to observe the dynamics of the domain, ^{15}N R_1, R_2, $R_{1\rho}$, and $^1H\rightarrow{}^{15}N$ nOe were measured at 30°C on a Bruker DRX-500 spectrometer, using the classical pulse programs [45, 46]. H-D exchange was followed during 48 hr by recording a series of "fast" ^{15}N-HSQC on a Bruker DRX-600 spectrometer.

Experimental Restraints

The volumes of the nOe crosspeaks were integrated. Calibration of these dipolar correlations was achieved on the basis of the known range of $d\alpha N$ distances. The errors made on the distances d were evaluated to 0.25d for unambiguous backbone-backbone effects and to $0.125d^2$ for the remaining effects. Backbone torsion angles were derived from backbone ^1H, ^{15}N, and ^{13}C chemical shifts using the program TALOS [21] and from the analysis of the HNHA experiment. An error of ±30° was allowed for all angle restraints. Hydrogen bonds were imposed in the β structure when the corresponding amide protons were still observed after 30 min in D_2O.

Structure Calculation

A semiautomated iterative assignment procedure was applied for the assignment of the nOes and the construction of the three-dimensional structures. This procedure is described in detail in Savarin et al. [47]. A force field adapted to NMR structure calculation (file topallhdg.pro and parallhdg.pro in X-PLOR 3.1) was used. At the last step, 500 structures were calculated and the best structures were selected and refined with a standard energy function (file topallh22x.pro and parallh22x.pro). The 15 best structures were selected for analysis. Structure figures were generated using the MOLMOL program [48].

Protection Factor Calculation

The intrinsic amide proton exchange rates were calculated using the method of Bai with the SPHERE program (HXPRED4-6, A. Robertson, P. Laub, Y.U. Zang, and H. Roder; http://www.fccc.edu/research/labs/roder/sphere [49, 50]). The protection factors P were calculated as k_{int}/k_{exp}, with k_{exp} being the experimental exchange rate and k_{int} the intrinsic exchange rate.

Circular Dichroism

The lamin C-terminal domain mutants were analyzed by circular dichroism using a Jobin Yvon CD6. Spectra were recorded between 190 and 300 nm on 1 ml protein samples (optical length: 1 cm) at a temperature varying from 10 to 90°C.

Acknowledgments

We thank Gérard Batellier, Roland Nageotte, and Michel Goldberg for the ultracentrifugation experiments and Nicolas Gilles for technical assistance during ^{15}N and ^{13}C labeling. Sébastien Foucher was helpful in analyzing the NMR relaxation data. Clinicians (Leila Akhmadeyeva, Jaume Colomer, Jean-François Forissier, Naomi Hino, Helen Kingston, Michel Komadja, Kayoko Saito, and John Yates) are sincerely thanked for providing samples from their patients for the *LMNA* mutation screening. Laurence Demay and Pascale Richard are thanked for their help in the *LMNA* mutation screening. Isabelle Callebaut is acknowledged for fruitful discussions. Françoise Ochsenbein is acknowledged for technical assistance during the CD experiments. H.J.W. is supported by grants from the Muscular Dystrophy Association. H.J.W. and G.B. are supported by grants from the Human Frontiers Science Program (grant #RGP0057/2001-M101). S.Z.-J., G.B., and J.-C.C. are supported by grants from Association Française contre les Myopathies (AFM, grant #8185). G.B. is

supported by the European Union Fifth Framework Program (Grant Myo-Cluster Euromen contract #QLG1-1999-00870). The 800 MHz spectrometer was procured with the help of Région Ile de France and Association pour la Recherche sur le Cancer.

Received: December 28, 2001
Revised: March 28, 2002
Accepted: April 4, 2002

References

1. Gotzmann, J., and Foisner, R. (1999). Lamins and lamin-binding proteins in functional chromatin organization. Crit. Rev. Eukaryot. Gene Expr. *9*, 257–265.
2. Cohen, M., Lee, K.K., Wilson, K.L., and Gruenbaum, Y. (2001). Transcriptional repression, apoptosis, human disease and the functional evolution of the nuclear lamina. Trends Biochem. Sci. *26*, 41–47.
3. Stuurman, N., Heins, S., and Aebi, U. (1998). Nuclear lamins: their structure, assembly, and interactions. J. Struct. Biol. *122*, 42–66.
4. Foisner, R. (1997). Dynamic organization of intermediate filaments and associated proteins during the cell cycle. Bioessays *19*, 297–305.
5. Collas, I., and Courvalin, J.-C. (2000). Sorting nuclear membrane proteins at mitosis. Trends Cell Biol. *10*, 5–8.
6. Andrulis, E.D., Neiman, A.M., Zappulla, D.C., and Sternglanz, R. (1998). Perinuclear localization of chromatin facilitates transcriptional silencing. Nature *394*, 592–595.
7. Mancini, M.A., Shan, B., Nickerson, J.A., Penman, S., and Lee, W.H. (1994). The retinoblastoma gene product is a cell cycle-dependent, nuclear matrix-associated protein. Proc. Natl. Acad. Sci. USA *91*, 418–422.
8. Imai, S., Nishibayashi, S., Takao, K., Tomifuji, M., Fujino, T., Hasegawa, M., and Takano, T. (1997). Dissociation of Oct-1 from the nuclear peripheral structure induces the cellular aging-associated collagenase gene expression. Mol. Biol. Cell *8*, 2407–2419.
9. Rao, L., Perez, D., and White, E. (1996). Lamin proteolysis facilitates nuclear events during apoptosis. J. Cell Biol. *135*, 1441–1455.
10. Gruenbaum, Y., Wilson, K.L., Harel, A., Goldberg, M., and Cohen, M. (2000). Review: nuclear lamins—structural proteins with fundamental functions. J. Struct. Biol. *129*, 313–323.
11. Worman, H.J., and Courvalin, J.-C. (2000). The inner nuclear membrane. J. Membr. Biol. *177*, 1–11.
12. Lin, F., and Worman, H.J. (1993). Structural organization of the human gene encoding nuclear lamin A and nuclear lamin C. J. Biol. Chem. *268*, 16321–16326.
13. Fisher, D.Z., Chaudhary, N., and Blobel, G. (1986). cDNA sequencing of nuclear lamins A and C reveals primary and secondary structural homology to intermediate filament proteins. Proc. Natl. Acad. Sci. USA *83*, 6450–6454.
14. Weber, K., Plessmann, U., and Ulrich, W. (1989). Cytoplasmic intermediate filament proteins of invertebrates are closer to nuclear lamins than are vertebrate intermediate filament proteins: sequence characterization of two muscle proteins of a nematode. EMBO J. *8*, 3221–3227.
15. Bione, S., Maestrini, E., Rivella, S., Mancini, M., Regis, S., Romeo, G., and Toniolo, D. (1994). Identification of a novel X-linked gene responsible for Emery-Dreifuss muscular dystrophy. Nat. Genet. *8*, 323–327.
16. Bonne, G., Di Barletta, M.R., Varnous, S., Becane, H.M., Hammouda, E.H., Merlini, L., Muntoni, F., Greenberg, C.R., Gary, F., Urtizberea, J.A., et al. (1999). Mutations in the gene encoding lamin A/C cause autosomal dominant Emery-Dreifuss muscular dystrophy. Nat. Genet. *21*, 285–288.
17. Bonne, G., Muchir, A., Helbling-Leclerc, A., Massart, C., and Schwartz, K. (2002). Clinical and genetical heterogeneity of laminopathies. Acta Myologica, in press.
18. Wilson, K.L., Zastrow, M.S., and Lee, K.K. (2001). Lamins and disease: insights into nuclear infrastructure. Cell *104*, 647–650.
19. Gaboriaud, C., Bissery, V., Benchetrit, T., and Mornon, J.-P. (1987). Hydrophobic cluster analysis: an efficient new way to compare and analyse amino acid sequences. FEBS Lett. *224*, 149–155.
20. Callebaut, I., Labesse, G., Durand, P., Poupon, A., Canard, L., Chomilier, J., Henrissat, B., and Mornon, J.-P. (1997). Deciphering protein sequence information through hydrophobic cluster analysis (HCA): current status and perspectives. Cell. Mol. Life Sci. *53*, 621–645.
21. Cornilescu, G., Delaglio, F., and Bax, A. (1999). Protein backbone angle restraints from searching a database for chemical shift and sequence homology. J. Biomol. NMR *13*, 289–302.
22. Bonne, G., Mercuri, E., Muchir, A., Urtizberea, A., Becane, H.M., Recan, D., Merlini, L., Wehnert, M., Boor, R., Reuner, U., et al. (2000). Clinical and molecular genetic spectrum of autosomal dominant Emery-Dreifuss muscular dystrophy due to mutations of the lamin A/C gene. Ann. Neurol. *48*, 170–180.
23. di Barletta, M.R., Ricci, E., Galluzzi, G., Tonali, P., Mora, M., Morandi, L., Romorini, A., Voit, T., Orstavik, K.H., Merlini, L., et al. (2000). Different mutations in the LMNA gene cause autosomal dominant and autosomal recessive Emery-Dreifuss Muscular dystrophy. Am. J. Hum. Genet. *66*, 1407–1412.
24. Brown, C.A., Lanning, R.W., McKinney, K.Q., Salvino, A.R., Cherniske, E., Crowe, C.A., Darras, B.T., Gominak, S., Greenberg, C.R., Grosmann, C., et al. (2001). Novel and recurrent mutations in lamin A/C in patients with Emery-Dreifuss muscular dystrophy. Am. J. Med. Genet. *102*, 359–367.
25. Kitagushi, T., Matsubara, S., Sato, M., Miyamoto, K., Hirai, S., Schwartz, K., and Bonne, G. (2001). A missense mutation in the exon 8 of lamin A/C gene in a Japanese case of autosomal dominant limb-girdle muscular dystrophy and cardiac conduction block. Neuromuscul. Disord. *11*, 542–546.
26. Cao, H., and Hegele, R.A. (2000). Nuclear lamin A/C R482Q mutation in Canadian kindreds with Dunnigan-type familial partial lipodystrophy. Hum. Mol. Genet. *9*, 109–112.
27. Shackelton, S., Lloyd, D.J., Jackson, S.N., Evans, R., Niermeijer, M.F., Singh, B.M., Schmidt, H., Brabant, G., Kumar, S., Durrington, P.N., et al. (2000). LMNA, encoding lamin A/C, is mutated in partial lipodystrophy. Nat. Genet. *24*, 153–156.
28. Speckman, R.A., Garg, A., Du, F., Bennett, L., Veile, R., Arioglu, E., Taylor, S.I., Lovett, M., and Bowcock, A.M. (2000). Mutational and haplotype analyses of families with familial partial lipodystrophy (Dunnigan variety) reveal recurrent missense mutations in the globular C-terminal domain of lamin A/C. Am. J. Hum. Genet. *66*, 1192–1198.
29. Vigouroux, C., Magre, J., Vantyghem, M.C., Bourut, C., Lascols, O., Shackleton, S., Lloyd, D.J., Guerci, B., Padova, G., Valensi, P., et al. (2000). Lamin A/C gene: sex-determined expression of mutations in Dunnigan-type familial partial lipodystrophy and absence of coding mutations in congenital and acquired generalized lipoatrophy. Diabetes *49*, 1958–1962.
30. Hegele, R.A., Cao, H., Anderson, C.M., and Hramiak, I.M. (2000). Heterogeneity of nuclear lamin A mutations in Dunnigan-type familial partial lipodystrophy. J. Clin. Endocrinol. Metab. *85*, 3431–3435.
31. Akke, M., Liu, J., Cavanagh, J., Erickson, H.P., and Palmer, A.G., Iii. (1998). Pervasive conformational fluctuations on microsecond time scales in a fibronectin type III domain. Nat. Struct. Biol. *5*, 55–59.
32. Bork, P., Holm, L., and Sander, C. (1994). The immunoglobulin fold. Structural classification, sequence patterns and common core. J. Mol. Biol. *242*, 309–320.
33. Halaby, D.M., and Mornon, J.-P. (1999). The immunoglobulin superfamily: an insight on its tissular, species, and functional diversity. J. Mol. Evol. *46*, 389–400.
34. Kelley, L.A., MacCallum, R.M., and Sternberg, M.J.E. (2000). Enhanced genome annotation using structural profiles in the program 3DPSSM. J. Mol. Biol. *299*, 499–520.
35. Berman, H.M., Westbrook, J., Feng, Z., Gilliland, G., Bhat, T.N., Weissig, H., Shindyalov, I.N., and Bourne, P.E. (2000). The Protein Data Bank. Nucleic Acids Res. *28*, 235–242.
36. Dechat, T., Korbei, B., Vaughan, O.A., Vlcek, S., Hutchison, C.J., and Foisner, R. (2000). Lamina-associated polypeptide 2α binds intranuclear A-type lamins. J. Cell Sci. *113*, 3473–3484.
37. Sakaki, M., Koike, H., Takahashi, N., Sasagawa, N., Tomioka,

S., Arahata, K., and Ishiura, S. (2001). Interaction between emerin and nuclear lamins. J. Biochem. *129*, 321–327.
38. Holt, I., Clements, L., Manilal, S., Brown, S.C., and Morris, G.E. (2001). The R482Q lamin A/C mutation that causes lipodystrophy does not prevent nuclear targeting of lamin A in adipocytes or its interaction with emerin. Eur. J. Hum. Genet. *9*, 204–208.
39. Sambrook, J., Fritsch, E.F., and Maniatis, T. (1989). Molecular Cloning: A Laboratory Manual (Cold Spring Harbor, NY: Cold Spring Harbor Laboratory Press).
40. Saiki, R.K., Gelfand, D.H., Stoffel, S., Scharf, S.J., Higuchi, R., Horn, G.T., Mullis, K.B., and Erlich, H. (1987). Primer-directed enzymatic amplification of DNA with a thermostable DNA polymerase. Science *239*, 487–491.
41. Östlund, C., Bonne, G., Schwartz, K., and Worman, H.J. (2001). Properties of lamin A mutants found in Emery-Dreifuss muscular dystrophy, cardiomyopathy and Dunnigan-type partial lipodystrophy. J. Cell Sci. *114*, 14435–14445.
42. Delaglio, F., Grzesiek, S., Vuister, G.W., Zhu, G., Pfeifer, J., and Bax, A. (1995). NMRPipe: a multidimensional spectral processing system based on UNIX pipes. J. Biomol. NMR *6*, 277–293.
43. Clore, G.M., and Gronenborn, A.M. (1991). Structures of larger proteins in solution: three- and four-dimensional heteronuclear NMR spectroscopy. Science *252*, 1390–1399.
44. Bax, A., and Grzesiek, S. (1993). Methodological advances in protein NMR. Acc. Chem. Res. *26*, 131–138.
45. Kay, L.E., Nicholson, L.K., Delaglio, F., Bax, A., and Torchia, D.A. (1992). Backbone dynamics of proteins as studied by ^{15}N inverse detected heteronuclear NMR spectroscopy: application to Staphylococcal nuclease. J. Magn. Res. *97*, 359–375.
46. Zinn-Justin, S., Berthault, P., Guenneugues, M., and Desvaux, H. (1997). Off-resonance rf fields in heteronuclear NMR: application to the study of slow motions. J. Biomol. NMR *10*, 363–372.
47. Savarin, P., Zinn-Justin, S., and Gilquin, B. (2001). Variability in automated assignment of NOESY spectra and three-dimensional structure determination: a test case on three small disulfide-bonded proteins. J. Biomol. NMR *19*, 49–62.
48. Koradi, R., Billeter, M., and Wuthrich, K. (1996). MOLMOL: a program for display and analysis of macromolecular structures. J. Mol. Graph. *14*, 51–55.
49. Bai, Y., Milne, J.S., Mayne, L., and Englander, S.W. (1993). Primary structure effects on peptide group hydrogen exchange. Proteins *17*, 75–86.
50. Connelly, G.P., Bai, Y., Jeng, M.F., and Englander, S.W. (1993). Isotope effects in peptide group hydrogen exchange. Proteins *17*, 87–92.
51. Altschul, S.F., Madden, T.L., Schaffer, A.A., Zhang, J., Zhang, Z., Miller, W., and Lipman, D.J. (1997). Gapped BLAST and PSI-BLAST: a new generation of protein database search programs. Nucleic Acids Res. *25*, 3389–3402.